Multifiber Deterministic Streamline Tractography of the Corticospinal Tract Based on a New Diffusion Model

Olivier Commowick, Aymeric Stamm, Romuald Seizeur, Patrick Pérez, Christian Barillot, Sylvain Prima, Nicolas Wiest-Daesslé

Multifiber Deterministic Streamline Tractography of the Corticospinal Tract Based on a New Diffusion Model

Olivier Commowick[1], Aymeric Stamm[1], Romuald Seizeur[1,3], Patrick Pérez[4], Christian Barillot[1], Sylvain Prima[1], and Nicolas Wiest-Daesslé[1,2]

[1] VISAGES: INSERM U746 - CNRS UMR6074 - INRIA - Univ. of Rennes I, France
[2] Department of Neurology, CHU Rennes, France
[3] Department of Neurosurgery, CHU Brest, France
[4] Technicolor, Rennes, France
Contact: Olivier.Commowick@irisa.fr

Abstract. In this paper, we build upon a new model, describing the random motion of water molecules in fibrous tissues, to develop a multifiber deterministic tractography algorithm. We apply this algorithm to track the corticospinal tract of the human brain, in both controls and patients with tumors.

1 Introduction

Tractography of the corticospinal tract (CST) using diffusion-weighted MRI (DW-MRI) is especially challenging, mostly due to the numerous fiber crossings in the corona radiata. When classical diffusion models (e.g. single or multiple tensors) coupled with simple tractography algorithms (e.g. deterministic streamline) are used, these crossings often make it impossible to track the most lateral fibers of the CST [1]. These include especially important motor areas such as the hand and the whole face, as shown by the homunculus of Penfield & Rasmussen. The fact that HARDI sequences are prohibitively time-consuming in case of patients with tumors makes it critically important to develop diffusion models and/or tractography algorithms able to track these lateral fibers from clinical (fast) diffusion sequences, having a small number of encoding gradients. We recently proposed a diffusion model that seems to meet these requirements even when using a simple deterministic streamline algorithm [2].

We briefly outline this new model in Section 2.1, the tractography algorithm in Section 2.2, and the pipeline we used to extract the CST in Section 2.3. Finally, we provide tractography results of the left and right CST on the two controls and two patients of the challenge dataset in Section 3.

2 Methods

2.1 Diffusion Modeling

In each voxel, water molecules are assumed to be distributed in several compartments. We first describe how we model the diffusion within a single compartment.

Then, we introduce our multi-compartment model, coined Diffusion Directions Imaging (DDI), and finally we outline how to estimate its parameters.

Single-compartment Model The diffusion process induces, after a diffusion time τ, a random displacement of water molecules from their initial position $\boldsymbol{x}_0$ to a random position $\boldsymbol{x} = \boldsymbol{x}_0 + \sqrt{2\tau}\boldsymbol{w}$. Assuming a **unique** direction of diffusion, we propose to model the random variable $\boldsymbol{w}$ as $\boldsymbol{w} = \boldsymbol{u} + \boldsymbol{v}$, where:

- $\boldsymbol{u}$ follows a **von Mises & Fisher** distribution parametrized by (i) the radius $R > 0$ of the sphere on which it is defined, (ii) the spherical coordinates (θ, ϕ) of its mean direction $\boldsymbol{\mu}$ and (iii) its concentration parameter $\kappa \geq 0$;
- $\boldsymbol{v}$ follows a **centered Gaussian** distribution parametrized by a cylindrically constrained [3] covariance matrix $D = \frac{R^2}{\kappa+1}\left(I + \kappa\boldsymbol{\mu}\boldsymbol{\mu}'\right)$, where I is the identity matrix and $\{\boldsymbol{\mu}, \kappa, R\}$ are the same parameters that characterize $\boldsymbol{u}$;
- $\boldsymbol{u}$ and $\boldsymbol{v}$ are statistically independent.

In essence, (i) $\boldsymbol{\mu}$ can be interpreted as the direction of the fibers which constrain the diffusion, (ii) R can be interpreted as the radial displacement along the fiber direction $\boldsymbol{\mu}$ and (iii) κ can be interpreted as a measure of anisotropy of the diffusion. The latter can be related to the fractional anisotropy (FA) [4] as $\mathrm{FA} = \kappa\left[(\kappa+1)^2 + 2\right]^{-1/2}$. We refer the reader to [2] for more details about the motivations of such a parametrization.

The probability density function (pdf) of the molecular displacement $\boldsymbol{x} - \boldsymbol{x}_0$ is then obtained by the convolution of the von Mises & Fisher pdf and the Gaussian pdf, and is parametrized by the four parameters $\{\theta, \phi, \kappa, R\}$.

Multi-compartment Model Due to its low number of parameters, the single-compartment model is particularly suited to be encompassed within a multi-compartment model, which can account for more than one fiber direction within each voxel. We thereby model the pdf of molecular displacements as a mixture of pdfs having the common parametric form proposed in the previous section.

We assume m compartments associated with m different fiber directions $\boldsymbol{\mu}_i$ $(i = 1, \ldots, m)$. In each compartment, the diffusion is modeled according to the previously described pdf with parameters $\{\boldsymbol{\mu}_i, \kappa_i, R_i\}$ and mixture weight FA_i/m. We also include an additional pdf in the mixture, with weight $1 - \sum_{i=1}^{m} \mathrm{FA}_i/m$ to account for isotropic diffusion; this pdf follows the general form with $\kappa = 0$, so that the unique remaining parameter to estimate is R_0. Furthermore, we set $R_i^2 = (\kappa_i + 1)\lambda$, $\forall i \in [\![1, m]\!]$, where $\lambda > 0$ is the transverse diffusivity assumed identical in each compartment. For more details about the above described parametrization, we invite the reader to see [2]. Considering m putative fiber directions with this parametrization yields a m-compartment DDI model with $3m + 1$ parameters.

Estimation of the DDI Parameters The theoretical diffusion weighted intensities are the modulus of the Fourier transform of the pdf of molecular displacements which can be analytically derived under the assumption of the DDI model

[2]. The $3m+1$ unknown parameters of the m-compartment DDI model are then **estimated** using a least squares fitting on the raw diffusion weighted intensities, and this **optimization** is performed using the derivative-free NEWUOA optimization algorithm [5]. The different compartments are sorted in decreasing order according to their κ. The model selection is performed according to the procedure described in [2].

2.2 Tractography Algorithm

Our goal is to track the fibers linking multiple regions of interest (ROIs). To this end, we developed a deterministic streamline algorithm, which can be viewed as an extension of the original FACT method [6], adapted to the DDI model, using a *breadth-first*-type search.

Starting from one of the ROIs, we define one starting point at each voxel of the ROI. Given one point along its path, we build the *main* fiber iteratively as follows:

1. If the number of putative fiber directions $m = 0$, we stop the tracking.
2. If $m = 1$, we compute FA_1 and the angle α_1 between the input direction and $\boldsymbol{\mu_1}$. If $\alpha_1 < \alpha_t$ and $\mathrm{FA}_1 > \mathrm{FA}_t$, then we follow the single putative fiber direction $\boldsymbol{\mu_1}$ with a step size of l millimeters. Else, we stop the tracking.
3. If $m = 2$, we compute FA_1, FA_2, the angle α_1 (resp. α_2) between the input direction and $\boldsymbol{\mu_1}$ (resp. $\boldsymbol{\mu_2}$). If:
   - $\alpha_t < \alpha_1, \alpha_2$: we stop the tracking.
   - $\alpha_1 < \alpha_t < \alpha_2$: cf. the case $m = 1$.
   - $\alpha_2 < \alpha_t < \alpha_1$: if $\mathrm{FA}_2 > \mathrm{FA}_t$, then we follow the direction $\boldsymbol{\mu_2}$ with a step size of l millimeters, else we stop the tracking.
   - $\alpha_1, \alpha_2 < \alpha_t$: if $\mathrm{FA}_2 < \mathrm{FA}_t$, then cf. the case $m = 1$; else if $\kappa_2 > r \times \kappa_1$ then we sort the two fibers in ascending order according to the angles α_i. We follow the new direction $\boldsymbol{\mu_1}$ with a step size of l millimeters and we record the second putative fiber direction $\boldsymbol{\mu_2}$ (*branch*) for future use, as it can be indicative of crossing/kissing/merging/diverging fibers.

Once we have tracked this main fiber, we perform the same tracking from all the possible branching points that we have recorded along its path. Importantly, for these trackings, the stepping rule and stopping criteria are identical as those for the main fiber, but we do not record any possible mixed fiber configuration along these secondary paths, for which we only follow the main direction $\boldsymbol{\mu_1}$ at each step. We then lead the same tracking from the other ROIs. We only keep the tracts going through all the seeding ROIs for further analysis. In practice, we choose the parameters $l = 1$, $r = 0.8$, $\alpha_t = 60$ degrees (maximal angle between two successive directions along the fiber) and $\mathrm{FA}_t = 0.5$ (minimal FA along the fiber). During the tracking, when a point is not on the grid of the DW-MR images, we compute the DDI model using a trilinear interpolation directly on the model parameters.

2.3 Tractography Pipeline Applied to the Challenge Datasets

We utilize the following processing pipeline to extract the CST for the challenge datasets. An expert neuroanatomist (Romuald Seizeur) delineated two ROIs on each side (left and right) of the original T1-weighted images. One is located in the posterior limb of the internal capsule and the other in the superior part of the mesencephalon. In addition, since crossing fiber tracts such as the association or commissural fiber tracts may be considered as bifurcations of the CST by the tractography algorithm, the same expert also delineated regions through which the tracts are not allowed. On the patients' datasets, the same ROIs were delineated with some modifications to account for the deformations caused by the tumor (e.g. in patient 1 the internal capsule on the left side is compressed by the infiltrating tumor).

All datasets were then processed in three steps:

1. Diffusion-weighted MRI denoising: DW-MRI is subject to random noise yielding measures that are different from their real values, and thus biasing the subsequently estimated diffusion models. We filtered the diffusion-weighted MR images with the Rician-adapted Non-Local Means filter [7], which has been shown to efficiently denoise such images while preserving fine anatomical structures. In particular, this filter has also been shown to preserve the angular resolution of q-ball ODF models estimated from HARDI data [8].
2. ROI alignment on B0 images: we registered the ROIs on the B0 images according to the following steps:
   - global affine registration of the T1-weighted images to the B0 images [9];
   - cropping of the affine-registered T1-weighted images using the mask of the B0 images;
   - constrained non-rigid registration [10] of the masked T1-weighted images to the B0 images;
   - application of the obtained transformations to the ROIs.
3. Extraction of the left and right CST using the aligned ROIs and the DDI estimated from the DWI.

3 Results

The MICCAI DTI tractography challenge consists of two groups of data: two healthy subjects acquired using a multiple b-values scheme and two patients acquired using a more standard acquisition protocol. For each of the two healthy subjects, DW-MRI data were acquired repeatedly (ten repetitions) so that the reproducibility of the tractography method may be evaluated. On the other hand, the tumors of the two patients were delineated so that we could produce combined views to help the surgeon, for example when planning a tumor removal surgery.

3.1 Tractography on Healthy Subjects

For each of the repetitions of each subject, the left and right CST were computed utilizing the aligned ROIs (see Section 2.3). We display the tractography of one volume of each of the two subjects in Fig. 1.

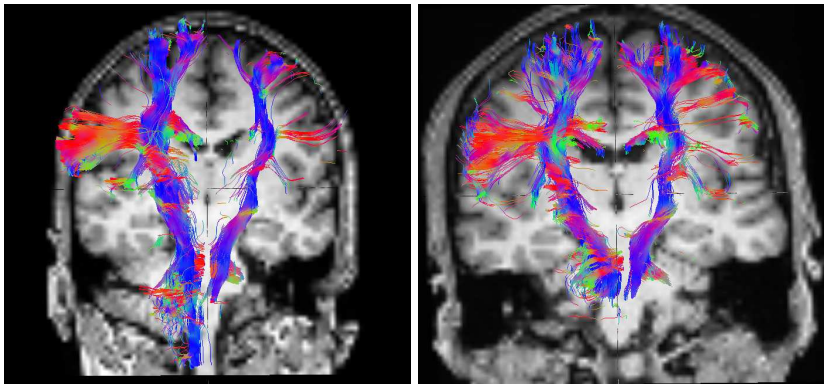

(a) (b)

Fig. 1. Illustration of CST on Healthy Subjects. Representative examples of obtained fiber tracts for healthy subject 1 (a) and 2 (b) (T1 images are in radiological conventions, i.e. the left hemisphere is on the right side of the image). To see the full extent of fiber spreading, all 3D fiber tracts are displayed. This explains why they may not seem to match exactly the background T1 image.

This figure illustrates that we are able to cover the full extent of the CST for these healthy subjects, from the face area to the hand area to the medial part of the CST. This demonstrates that our diffusion model enables the tractography algorithm to follow bifurcations in the white matter fiber tracts. For each subject, estimating the DDI models from the DWI took approximately 40 minutes (single-threaded), while the tractography of the left and right CST took less than ten minutes.

3.2 Tractography on Patients

We also report results for the CST of each patient on the side of the tumor (all fiber bundles are provided in supplemental material). The images processed here had a larger resolution than the healthy subjects and the estimation of the DDI models from the DWI took approximately 3 hours (single-threaded). However, this step of the tractography pipeline may be computed offline leaving only the tractography to perform online (about five minutes for each CST) when performing the tractography for surgery planning.

We focus on the qualitative evaluation of the obtained tracks and their closeness to the tumor (it should be noted that the tumor regions were not used in

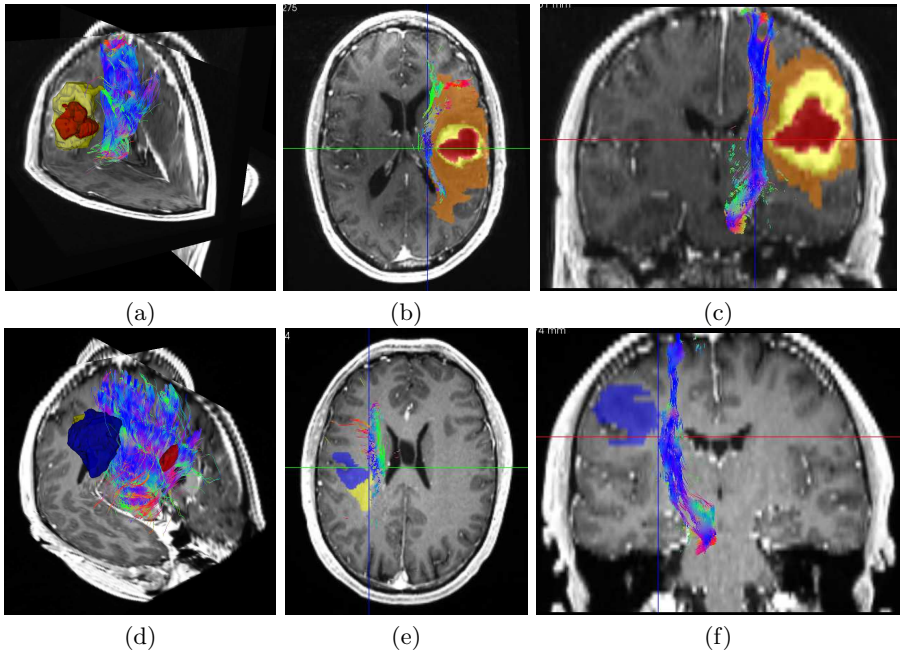

Fig. 2. Illustration of CST on Patients. Combined views of the obtained fiber tracts for patients 1 (a,b,c) and 2 (d,e,f), illustrating the proximity of the tumor to crucial motor pathways. Surfaces for the first patient correspond to the necrotic part of the tumor (red), the active part of the tumor (yellow) and the edema (orange). For the second patient, each ROI corresponds to a specific tumor. Images (a,d) show overall 3D views and (b,c,e,f) show the tracts and regions of interest going through a specific 2D slice to better illustrate their proximity.

any way to constrain the tractography algorithm), and on providing the neurosurgeon with helpful views for neurosurgery planning. To this end, we present in Fig. 2 views (made using the MedINRIA software [11]) combining the fiber tracts, the tumor ROIs provided by the organizers, all on top of the patient's T1 image. More illustrations are available in supplemental material.

We can observe on this figure that, although the tumor delineation was not used in the algorithm, no fibers are going through the tumor area on patient 1. Instead, the CST is going through the most central part of the edema (see images (b,c) on Fig. 2). This indicates that the fibers were pushed by the tumor mass effect, which is a valuable indication when planning the surgery. Overall, this figure demonstrates the close proximity of the tumors and of the CST for both patients. This is an important insight as the neurosurgeon will be able to plan the tumor removal in the optimal way, so as to minimize the possible handicap for the patient after surgery.

Acknowledgments This investigation was partly supported by the ARSEP (French MS society, Fondation pour l'Aide à la Recherche sur la Sclérose en Plaques).

References

1. Behrens, T.E.J., Berg, H.J., Jbabdi, S., Rushworth, M.F.S., Woolrich, M.W.: Probabilistic diffusion tractography with multiple fibre orientations: What can we gain? Neuroimage **34**(1) (January 2007) 144–155
2. Stamm, A., Pérez, P., Barillot, C.: Diffusion directions imaging. Research Report RR-7683, INRIA (2011)
3. Friman, O., Westin, C.F.: Uncertainty in white matter fiber tractography. In: MICCAI. (2005) 107–14
4. Basser, P.J., Pierpaoli, C.: Microstructural and physiological features of tissues elucidated by quantitative-diffusion-tensor MRI. Journal of magnetic resonance. Series B **111**(3) (June 1996) 209–19
5. Powell, M.: The NEWUOA software for unconstrained optimization without derivatives. In Pardalos, P., Pillo, G., Roma, M., eds.: Large-Scale Nonlinear Optimization. Volume 83 of Nonconvex Optimization and Its Applications. Springer US (2006) 255–297
6. Mori, S., Crain, B.J., Chacko, V.P., van Zijl, P.C.: Three-dimensional tracking of axonal projections in the brain by magnetic resonance imaging. Ann Neurol **45**(2) (February 1999) 265–269
7. Wiest-Daesslé, N., Prima, S., Coupé, P., Morrissey, S.P., Barillot, C.: Rician noise removal by non-local means filtering for low signal-to-noise ratio MRI: applications to DT-MRI. In: MICCAI, New York, United States (2008) 171–9
8. Descoteaux, M., Wiest-Daesslé, N., Prima, S., Barillot, C., Deriche, R.: Impact of Rician Adapted Non-Local Means Filtering on HARDI. In: MICCAI. (2008) 122–30
9. Ourselin, S., Roche, A., Prima, S., Ayache, N.: Block matching: A general framework to improve robustness of rigid registration of medical images. In: MICCAI. (2000) 557–66
10. Garcia, V., Commowick, O., Malandain, G.: A Robust and Efficient Block Matching Framework for Non Linear Registration of Thoracic CT Images. In: MICCAI'2010 Grand Challenges in Medical Image Analysis Workshop. (2010)
11. Toussaint, N., Souplet, J., Fillard, P.: MedINRIA: Medical Image Navigation and Research Tool by INRIA. In: MICCAI'2007 Workshop on Interaction in Medical Image Analysis and Visualization. (2007)